Theoretical and Experimental Results for Multipactor Effect in Groove Gap Waveguide Bandpass Filters with Inductive Coupling Irises

Alejandro Jorge-López[(1)], José Joaquín Vague[(1)], Irene Asensio[(1)], Ángela Coves[(2)], Ángel A. San Blas[(2)], Mariano Baquero-Escudero[(1)], Máriam Taroncher[(1)], Ana Vidal[(1)], and Vicente E. Boria[(1)].

[(1)] ***Departamento de Comunicaciones-ITEAM,***
Universitat Politècnica de València, 46022 Valencia, Spain
E-mail: ajorlop@iteam.upv.es, vboria@dcom.upv.es

[(2)] ***Department of Communications Engineering-I3E,***
Universidad Miguel Hernández de Elche, 03202 Elche, Spain

ABSTRACT

This article presents the theoretical study and experimental validation of the multipactor (MP) effect in bandpass filters implemented in groove gap waveguide (GGW) technology. Such filters are based on inductive coupling irises and rectangular cavities, whose optimized dimensions (widths and lengths) are fixed between rows of metal pins. For validation and comparative purposes, experimental results for both the GGW and its counterpart realized in standard rectangular waveguide (RW) technology, are included. For the effective design of the considered GGW filter, an equivalent counterpart in standard RW technology will be first studied, using very efficient tools for computing its electrical response and MP discharge breakdown level. Both filter prototypes, designed to operate at 17.5 GHz (for Ka-band satellite downlink applications), are made of aluminium, whose properties (in terms of secondary electron emission) have been measured and duly considered in their theoretical analysis (of multipactor breakdown thresholds) using available software tools. An outstanding matching between all predicted and experimental results is achieved.

I. INTRODUCTION

Multipactor (MP) is a potentially harmful discharge effect that occurs inside microwave components operating under high-vacuum conditions. In these situations, electrons allocated inside the device can be accelerated by electromagnetic (EM) fields of high amplitude (power level), pushing them (in a synchronized way) towards the surrounding surfaces, where they may impact with enough energy to extract more (and more) secondary electrons [1], [2]. If all these conditions are fulfilled, an electron chain discharge effect is produced inside the component, whose features (intensity and dynamics) strongly depends on the surface material property known as the Secondary electron Emission Yield (SEY) [3]. The resonant discharge inside the MP-affected component creates an electrical short-circuit that generates signal harmonics, decreases the signal-to-noise ratio (SNR) and, eventually, causes physical damages [4]–[6]. Thus, MP discharges have a great impact in many practical applications dealing with high-power microwave signals inside high-vacuum operating components, as it occurs in the output stage of satellite communication payloads [7]–[9] and in particle accelerators [10].

As it is well known [1], [2], the MP breakdown power (or MP threshold level) is directly related to the product of the operating frequency f (in GHz), and the gap distance d (in mm) between two surfaces of the microwave component. This dependence is clearly observed in the corresponding MP susceptibility charts, that were firstly obtained for parallel-plate waveguide geometries using analytical models [1] and empirical data [11]. Later on, several methods have been used for the study of the MP effect in widely common high-frequency technologies [12]–[16]. More recently, in order to estimate the MP threshold levels of advanced microwave hardware used in real applications, fast approximate techniques based on equivalent circuits, as well as on more accurate (and time-consuming) simulators for particles driven by EM fields, are also being employed [17].

A general trend in satellite applications is to increase the channel bandwidth (in order to support greater transmission rates), thus leading to higher operational frequencies. Indeed, this is the case of the high throughput satellite

This work has been funded by the Ministerio de Ciencia, Innovacion y Universidades (Spanish Government) through the Subprojects C41 and C43 of the R&D Projects PID2022-136590OB (under grant AEI/10.13039/501100011033/FEDER, UE) and TED2021-129196B (under grant 10.13039/501100011033/Unión Europea NextGenerationEU/PRTR), and in part by Conselleria de Educación, Universidades y Empleo, Generalitat Valenciana under Project CIAICO/2021/055.

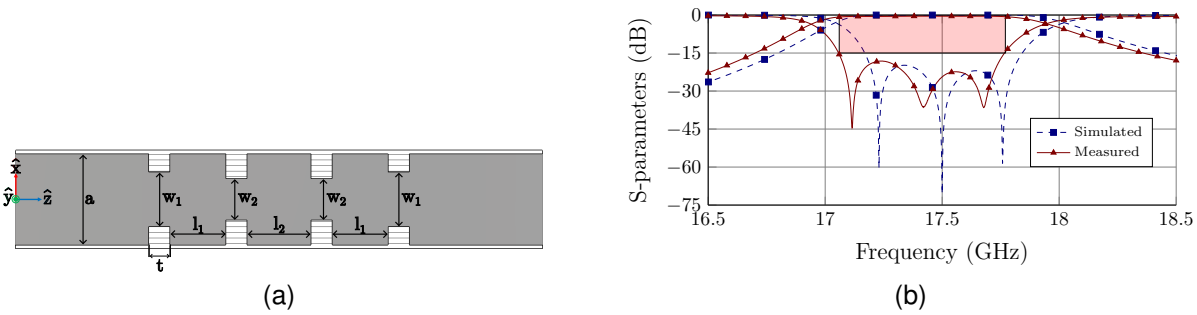

(a) (b)

Fig. 1: Geometry (top-view) in (a), and simulated and measured electrical response (S-parameters) in (b) of an inductive filter in RW technology (a= 12.95 mm, w_1= 7.73 mm, w_2= 5.86 mm, l_1= 8.05 mm, l_2= 9.18 mm and t= 3 mm, for a bandpass response of center frequency 17.5 GHz and relative bandwidth 3.85%). The height of the structure is 6.477 mm (for WR-51 ports) and 3 mm (for the optimal solution).

(HTS) systems [18], [19]. A recently emerged technology for the practical implementation of the involved high-frequency components, relies upon the use of groove gap waveguides (GGWs) [20], as recently demonstrated in [21]–[25] with several filters and diplexers. In this GGW solution, the tight metallic contact between the top lid and the body, which is always required when using the standard rectangular waveguide (RW) technology, is widely relaxed. To this end, periodic rows of pins are used in the GGW body to provide a high-impedance condition to the top lid, so the cited perfect metallic contact is not anymore needed [26]–[28].

However, real components may suffer from high-power discharges (in particular MP breakdown) within the cited tiny gaps between metallic surfaces (top cover and body), thus limiting their power-handling capabilities. Nevertheless, and so far, there are only two very recent contributions addressing the problem of electronic discharges in GGW technology [29], [30]. Therefore, there is a complete lack of theoretical and experimental studies of the MP effect in GGW filters, which are aimed to be fully addressed in this article. A comparison of the GGW filter results with those for a counterpart in standard RW technology is also performed, in order to confirm they can be alternative technological solutions.

In this paper, we will consider a GGW filter (with a bandpass response of 675 MHz centered around 17.5 GHz) based on cavities coupled through inductive irises. For its complete design process (both in terms of electrical response and MP effect), the filter counterpart in RW technology will be first studied, using efficient software tools based on modal analysis and MP theoretical models specially suited for RW geometries. Proceeding in this way, the maximum value of the filter height (compatible with the MP breakdown power levels that can be measured in the available experimental facility) will be found, hence also considering a more realistic component in terms of GGW height. The next sections of this paper cover all cited contents related to the electrical design, and MP effect analysis, of the proposed GGW filter and its RW counterpart. Experimental results for both filter prototypes, obtained from a test campaign performed at the High Power Laboratories of the European Space Agency (ESA) and the Val Space Consortium (VSC) [31], are compared and properly discussed. Finally, the main conclusions of this work are briefly outlined.

II. MULTIPACTOR ANALYSIS OF INDUCTIVE FILTERS IN RECTANGULAR WAVEGUIDES

Inductively-coupled RW filters are based on the cascade connection of RWs (all with the same height, but with different width values), whose geometry (top-view) can be seen in Fig. 1a. For this work, a third-order RW filter, with a Chebyshev response centered at 17.5 GHz (Ka-band) with a relative bandwidth of 3.85% (around 675 MHz), has been designed using the automatic synthesis tool of FEST3D (CST Studio Suite, Dassault Systèmes [32]). The resulting dimensions of such RW filter are included in the caption of Fig. 1, whereas its simulated electrical response (matching the required specifications) is shown in Fig. 1b.

The filters are fed with a standard WR-51 (of size 12.954 mm $\times$ 6.477 mm). For such a nominal height value (i.e. 6.477 mm), the MP breakdown power levels will be of several tens of kW (well beyond the maximum value available in the experimental facility [31], which is around 5 kW for the considered Ka-band frequency range). Thus, the height value must be properly reduced. For this purpose, an effective iterative procedure (based on very efficient MP analysis models) will be used to find the optimal height solution.

We can see in Fig. 2 that the maximum value of the electric field magnitude is located in the center of the second (central) cavity. Due to the particular geometry of inductive filters (invariant with height), the pattern for the electric field

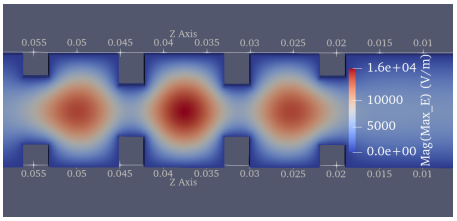

Fig. 2: Electric field distribution in the RW inductive filter computed at 17.5 GHz (with levels scaled for an input power level of 1 W and a height of 6.477 mm).

distribution is kept constant for any height value. Therefore, the same location for having a MP discharge can be considered in the iterative design process of the filter height.

We will first compute the MP threshold power of a uniform section of the RW implementing the central cavity (P_{TH}), using a MP analysis tool based on the effective-electron model, originally developed and validated in [33], [34] (Numerical-RW). Additionally, a simplified version of the previous tool (based on the analytical resolution of the effective electron trajectory) has also been developed for this work (Analytical-RW). Even though both models can solve the MP discharge effect in empty RWs very efficiently, the second version is extremely fast, and particularly suitable for the proposed procedure. It is based on neglecting the influence of the magnetic field components of the RW fundamental mode, valid when calculating electron trajectories under non-relativistic velocities, which is the usual case in microwave hardware for satellite applications, so that the resolution of the effective electron trajectory is analytical.

We can easily relate the previously computed P_{TH} value with the peak voltage level (V_{TH}) required for such a discharge, using the well-known relationship [17]:

$$V_{TH} = V_{1W} \sqrt{\frac{P_{TH}}{P_{1W}}} = V_{1W} \sqrt{P_{TH}} \tag{1}$$

where V_{1W} is the peak voltage in the critical gap of the uniform RW (which is located at the waveguide center, where the TE_{10} mode electric field is maximum), for a mean power level of 1 W at the waveguide input port (P_{1W}= 1 W). However, we finally need to know the MP threshold power at the input port of the whole inductive filter (P_{FTH}), that will be lower than the previous one (P_{TH}) due to the voltage magnification effect originated in the resonant cavities of bandpass filters [7]. In this case, we can easily compute the value of P_{FTH} as follows:

$$P_{FTH} = P_{F1W} \left(\frac{V_{TH}}{V_{F1W}}\right)^2 = P_{TH} \left(\frac{V_{1W}}{V_{F1W}}\right)^2 \tag{2}$$

where V_{F1W} is the value of the peak voltage in the middle of the central resonant cavity of the filter for a 1 W mean power level at the filter input port (P_{F1W}= 1 W). It must be noted that the values of V_{1W} and V_{F1W} are also efficiently computed with the software tool FEST3D. Applying this procedure to our case, iteratively, an optimal value of 3 mm for the RW filter height is found after completing few simple steps.

Next, we will check that the two efficient MP analysis tools used in this work (the Numerical-RW and the Analytical-RW ones) do also provide accurate results. For this purpose, we have first considered a uniform RW section of size 12.954 mm × 3 mm, made of aluminium material (whose standard SEY data, from [35] and compiled in Tab. I, are used). For validation of the P_{TH} values obtained for the cited RW, we have also used the well-known software tool SPARK3D (v. 2023, Dassault Systèmes), based on a more elaborated algorithm for tracking electrons driven by the real EM fields inside the component. In order to get the results, 10 000 initial electrons were homogeneously distributed within the uniform RW section, thus involving 24 hours for the complete simulation of MP effect at each frequency point. This extremely large computational effort is directly related to the very high order of the MP mode excited in the uniform RW (that SPARK3D has predicted to be equal to 73), as it can be expected for a value of the frequency-gap product ($f \times d$) of 52.5 GHz × mm, considering the central frequency of 17.5 GHz.

Using the two efficient tools for the MP effect analysis, properly configured as detailed next, we have also computed a very close value (of 71) for the order of the excited discharge mode. These results confirm that a large number of half-cycles of the sinusoidal excitation signal must be considered to reach reliable MP results. Thus, longer temporal simulation intervals will be involved, which discourages the use of very accurate (but less computationally efficient) commercial tools in this case. Both the Numerical-RW and the Analytical-RW tools have computed the P_{TH} values of Fig. 3a following the same statistical approach. For each power value, the trajectories of 36 effective electrons, with initial

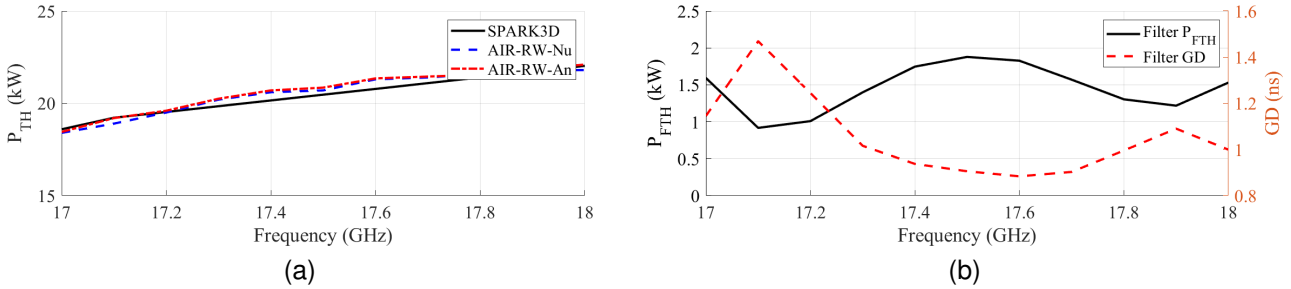

Fig. 3: P_{TH} for the WR-51 RW with a height of 3 mm, computed with SPARK3D (solid line) and with the two efficient MP tools for RWs (Numerical-RW and Analytical-RW with dashed and dotted lines) in (a), and P_{TH} of the filter in WR-51 RW with a height of 3 mm (P_{FTH}, left-hand side scale), and filter group delay (GD, right-hand side scale), computed with the Analytical-RW tool (P_{TH} values) and FEST3D, respectively, in (b).

TABLE I: Standard and measured SEY data for aluminium (Al) material.

Material	E_{max} (eV)	E_1 (eV)	δ_0	δ_{max}
Al (ECSS2020 [35])	276.000	17.000	0.800	2.920
Al (measured)	246.500	16.154	0.903	2.485

phases of the driving electric field uniformly distributed between 0° and 360°, are computed. They are launched from the center of the RW, and from random positions between y = -1.5 mm and y = 1.5 mm. After 300 periods ($T = 1/f$) of the high-frequency excitation signal, for all simulated trajectories, the average value of the final population of electrons (N) is used to determine (if such a value is above 1) that a MP discharge has occurred. It is important to note that the results obtained with the Analytical-RW tool were computed in just 2 minutes per frequency point, while those provided by the Numerical-RW approach took 55 minutes per frequency point. Fig. 3a shows the three sets of previous results for 11 points in the frequency range from 17 GHz to 18 GHz (where the whole pass-band of the RW inductive filter is included). As can be seen, a very good agreement between all MP results is achieved.

Next, using the values of P_{TH} provided by the Analytical-RW tool (see Fig. 3a) in (2), together with figures for V_{1W} and V_{F1W} computed before, we have finally estimated the levels of P_{FTH} of the RW inductive filter, shown in Fig. 3b, which confirm that all values of P_{FTH} for the selected optimal height (i.e. 3 mm) remain below the maximum breakdown level occurring at 17.5 GHz (the filter center frequency) and, therefore, it is suitable for performing MP measurements in the selected facility. As can be seen, the minimum values of P_{FTH} are coincident with the peaks (maximums) of the filter GD (where the time-averaged stored energy (TASE) in the filter structure is also maximized) [17]. Finally, we have computed the value of P_{FTH} for the RW filter (at 17.5 GHz) using the accurate commercial tool SPARK3D which predicts a value of 3093 W for P_{FTH} (higher than the maximum value at 17.5 GHz in Fig. 3b, but still distant enough from the 5 kW limit of the experimental facility).

III. MULTIPACTOR ANALYSIS OF INDUCTIVE FILTERS IN GROOVE GAP WAVEGUIDES

Once the RW inductive bandpass filter has been deeply studied, we will proceed with its practical implementation in GGW technology (see the 3-D view of the proposed topology in Fig. 4a), and the corresponding MP analysis. For these purposes, more accurate (but less efficient) software tools (such as the high-frequency EM simulation solver of the aforementioned CST Studio Suite [32], and the electrons tracking code SPARK3D) will be needed to cope with the more intricated GGW geometry. To alleviate the corresponding computational burdens, we will rely on the available RW inductive solution as it is described next.

First, each RW (with the optimal height of 3 mm found in section II) of the inductive filter is directly replaced with its corresponding GGW counterpart (whose geometrical details are given in Fig. 4b). Regarding the periodic bed of pins (of square cross-section with size l_p separated a distance equal to s_p, see Fig. 4b), it has been properly designed for implementing the high-impedance surface of the GGW technology, thus obtaining l_p= 1.02 mm and s_p= 0.96 mm for a nominal height value of H_p= 6.477 mm and a = 12.95 mm. Such a textured surface, together with the top metal lid, prevent any potential leakage of EM energy through the GGW lateral sides [26], [27]. In this work, the zero-gap GGW realization (with H_A in Fig. 4b ideally equal to 0 μm) is used. The zero-gap solution is very convenient to avoid undesired MP discharges that, as thoroughly studied with uniform GGW sections [30], can be easily triggered at very low power

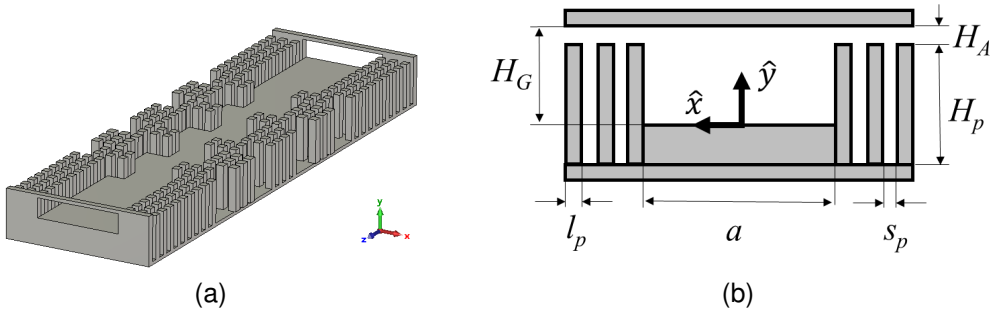

Fig. 4: 3-D view of the inductive bandpass filter in GGW technology in (a), and 2-D geometrical representation of each GGW in (b)

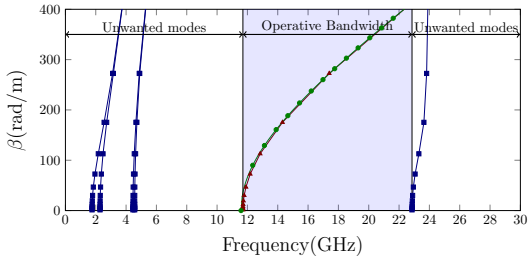

Fig. 5: Dispersion diagram of the GGW with size 12.954 mm × 3 mm, pins of l_p= 1.02 mm, s_p= 0.96 mm and H_A= 20 μm (unwanted modes with solid lines and fundamental mode with triangles marks), and of the equivalent RW (fundamental mode with circle marks).

TABLE II: Optimized values for dimensions (all in mm) of the RW and GGW inductive filters.

Dimension	a	w_1	l_1	w_2	l_2	t
RW	12.95	7.73	8.05	5.86	9.18	3.00
GGW	12.95	7.71	7.89	5.80	9.07	3.00

levels in the cited larger air gaps of the classical GGW case. However, due to mechanical tolerances, very small air gaps ($H_A \leqslant 20\,\mu$m) may be present in the produced pieces. Therefore, it has to be verified that such more realistic GGWs do not deviate (in terms of electrical response and MP discharge) from the ideal zero-gap case.

For this purpose, the dispersion diagrams of both waveguide implementations (in particular those of size 12.954 mm × 3 mm, used in the ports and resonant cavities of the two filters, and with $H_A = 20\,\mu$m for the GGW real version) are computed using the eigenmode solver of CST Studio Suite. As can be seen in Fig. 5, apart from some additional unwanted modes that appear in the GGW case (e.g. the ones at low frequencies due to the small, but non-zero, value of 20 μm considered for H_A), both fundamental modes do have overlapped dispersion responses in the same operational bandwidth. Thus, the proposed replacement of each RW in the original filter by its corresponding GGW implementation (with $H_A \leqslant 20\,\mu$m), is well justified in the single-mode frequency range of both waveguides.

In terms of the MP discharge, an empirical verification that such effect will not be produced (with very low power levels) in the cited small air gaps (of height values $H_A \leqslant 20\,\mu$m), is performed using the well-known susceptibility charts of parallel-plate geometries. For the considered range of realistic values for H_A, and at frequencies in the operational bandwidth of the GGW filter (below 18 GHz), the frequency-gap product ($f \times d$) will always meet that $f \times d \leqslant 0.36\,\text{GHz} \times \text{mm}$. Based on the standard susceptibility charts for aluminium material [11], and for such low values of the $f \times d$ term, it can be noticed that no MP discharge (of any order) will ever occur. As a result, we can also replace RWs by real GGW realizations (with $H_A \leqslant 20\,\mu$m) without affecting the MP response of the inductive filter.

It is an optimal choice to use, as initial values for all dimensions of the GGW filter to be designed, those found for the RW case (whose data are compiled in the first row of Tab. II). Proceeding in this way, and supported by CST Filter Designer 3D tool (also part of CST Studio Suite), the entire design process of the inductive bandpass filter in zero-gap ($H_A = 0\,\mu$m) GGW technology is completed after few steps. All geometrical dimensions involved at the filter design stage are shown in Fig. 6a, where it can be seen that most of the pins are those used before in the GGW body (i.e. with $l_{p1} = l_p = 1.02$ mm and $s_{p1} = s_p = 0.96$ mm), whereas the lateral pins of the first and third filter cavities do

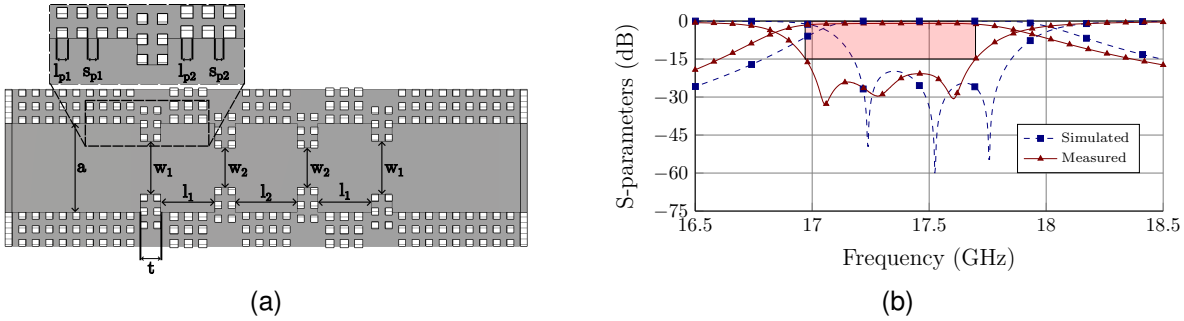

(a) (b)

Fig. 6: Geometry (top-view) in (a), and simulated and measured electrical response (S-parameters) in (b) of the inductive filter in GGW technology and height H_G= 3 mm.

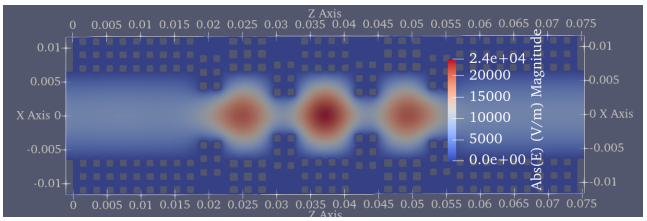

Fig. 7: Electric field distribution in the GGW inductive filter, calculated at 17.5 GHz (with levels scaled for an input power level of 1 W and height H_G= 3 mm).

TABLE III: Simulated (SPARK3D) and measured results (MP threshold levels) for RW and GGW filters at 17.4 GHz.

Model - Experiment	MP threshold (W)
RW simulation (ECSS2020 SEY)	3023.35
RW simulation (measured SEY)	3445.23
RW MP test	3424.50
GGW simulation (ECSS2020 SEY)	3163.98
GGW simulation (measured SEY)	3679.61
GGW MP test	3468.30

have l_{p2} = 1.2 mm and s_{p2} = 0.9 mm to best fit the requested optimal value for the length of such two resonators. A satisfactory bandpass response, fully compliant with the filter specifications in terms of central frequency and bandwidth, is also achieved (see Fig. 6b). These results also remain stable if some tiny air gaps were present (due to minor fabrication errors) above the metallic pins. Finally, the predicted value for the MP threshold power of the GGW filter (computed using SPARK3D) is 3188 W, which is very close (slightly higher) to the result for the equivalent RW filter (of 3093 W, as stated in section II), but also below the 5 kW limit of the experimental facility.

IV. EXPERIMENTAL RESULTS AND DISCUSSION

The two RW and GGW filters designed before (section II and section III) have been manufactured in aluminium, using an in-house computer numerical control (CNC) milling technique. Both filter implementations consist of a body and a smooth top metal lid. In order to measure the two fabricated filters, since their input and output ports have a height of 3 mm, E-plane tapered transformers to standard WR-51 RWs (with a height value of 6.477 mm) have been designed and built [36]. Comparisons between the simulated and measured results of the electrical response of the RW and GGW filter prototypes are shown in Fig. 1b and Fig. 6b, respectively. There is a frequency shift of 170 MHz (below 1% in relative terms) between simulated and measured GGW filter responses, which can be attributed to manufacturing tolerances (of 20 μm). Nevertheless, since the measured return loss levels are below 15 dB in the slightly shifted in-band responses, it will be possible to perform the MP study (analysis and, in particular, testing) of both filter units. In this case, such results will be obtained at the frequency of 17.4 GHz, where the pass-bands of the two fabricated prototypes are actually centered. The corresponding experimental SEY data have been obtained, from one metallic top lid of the filters, through measurements performed at the European High Power Space Materials Laboratory [31] (see Tab. I in section II).

For validation purposes, a MP test campaign (of both RW and GGW filter prototypes) was completed at the

European High Power RF Space Laboratory [31]. As can be seen in Tab. III, the MP threshold simulated results (using the experimental SEY data) are remarkably similar to the corresponding measured data. It must be also noted that the MP experimental results are also very close for both technological realizations (RW and GGW) of the considered inductive filters.

V. CONCLUSIONS

In this work, a comparative study (based on theoretical and experimental results) of the MP effect for inductively coupled bandpass filters, realized in RW and GGW technologies, is fully detailed. For that purpose, two filter units operating in the frequency range (17-18 GHz) planned for Ka-band satellite communications have been considered. For the effective design of the RW and GGW filters, meeting realistic size and electrical specifications together with measurable MP breakdown levels, very efficient modeling tools of such a discharge effect in RWs have been successfully applied. Then, more accurate results validating the MP response of the two given filter geometries, have been computed with SPARK3D.

The measured results for MP threshold values in both RW and GGW filter samples, are very similar to those predicted by precise simulators incorporating the experimental SEY data. Thus, an important conclusion is reached on the relevance of using real SEY data for the employed material, which allows a very accurate modelling of the MP discharge effect with available software products. Another major outcome of the study performed (fully validated with experimental data of real hardware), is that bandpass filters properly realized in the zero-gap GGW technology have very large MP threshold power levels. In fact, such results are shown to be very close to those of the equivalent -same height- RW counterpart, thus confirming the practical use of GGW filters in real space applications operating at the most challenging Ka-band frequency range.

ACKNOWLEDGEMENT

The authors would like to thank ESA and VSC, for contributing with its installations—cofunded by the European Regional Development Fund—a way of making Europe [31].

References

[1] A. J. Hatch and H. B. Williams, "Multipacting modes of high-frequency gaseous breakdown," *Phys. Rev.*, vol. 112, pp. 681–685, Nov. 1958.

[2] J. R. M. Vaughan, "Multipactor," *IEEE Trans. Electron Devices*, vol. 35, no. 7, pp. 1172–1180, Jul. 1988.

[3] J. R. M. Vaughan, "A new formula for secondary emission yield," *IEEE Trans. Electron Devices*, vol. 36, no. 9, pp. 1963–1967, Sep. 1989.

[4] W. C. Tang and C. M. Kudsia, "Multipactor breakdown and passive intermodulation in microwave equipment for satellite applications," in *Proc. IEEE Conf. Mil. Commun.*, Oct. 1990, pp. 181–187.

[5] M. Jimenez, B. Gimeno, C. Miquel-Espanya, *et al.*, "Analysis of the electromagnetic radiation generated by a multipactor discharge occurring within a microwave passive component," *J. Phys. D, Appl. Phys.*, vol. 43, no. 39, Oct. 2010, Art. no. 395501.

[6] D. Raboso, "Introduction to high power RF breakdown effects and PIM," in *Proc. Workshop High Power RF Breakdown PIM Space Appl., 48th Eur. Microw. Conf.*, Madrid, Spain, Sep. 2018.

[7] R. J. Cameron, C. M. Kudsia, and R. R. Mansour, *Microwave Filters for Communication Systems: Fundamentals, Design, and Applications*, 2nd ed. Hoboken, NJ, USA: Wiley, 2018.

[8] J. Uher, J. Bornemann, and U. Rosenberg, *Waveguide Components for Antenna Feed Systems: Theory and CAD*. Artech House, 1993.

[9] D. Raboso, "Multipactor effect on board spacecrafts: Present situation, future research activities and testing capabilities at the European Space Agency," in *Proc. Int. Vacuum Electronics Conf.*, 2000, pp. 14.2–14.4.

[10] J. Galarza, J. Navaridas, J. Pascual, T. Romero, J. Muñoz, and I. Bustinduy, "Parallelizing multipacting simulation for the design of particle accelerator components," in *2023 31st Euromicro Int. Conf. on Parallel, Distributed and Network-Based Process (PDP)*, 2023, pp. 149–153.

[11] A. Woode and J. Petit, "Diagnostic investigations into the multipactor effect, susceptibility zone measurements and parameters affecting a discharge," ESA/ESTEC, Noordwijk, The Netherlands, Work. Paper 1556, Nov. 1989.

[12] V. E. Semenov, E. I. Rakova, D. Anderson, M. Lisak, and J. Puech, "Multipactor in rectangular waveguides," *Phys. Plasmas*, vol. 14, no. 3, Mar. 2007, Art. no. 033501.

[13] A. M. Pérez, V. E. Boria, B. Gimeno, S. Anza, C. Vicente, and J. Gil, "Multipactor analysis in circular waveguides," *J. Electromagn. Waves Appl.*, vol. 23, no. 11–12, pp. 1575–1583, 2009.

[14] D. Gonzalez-Iglesias, P. Soto, S. Anza, *et al.*, "Multipactor susceptibility charts for ridge and multiridge waveguides," *IEEE Trans. Electron Devices*, vol. 59, no. 12, pp. 3601–3607, Dec. 2012.

[15] A. M. Perez, C. Tienda, C. Vicente, *et al.*, "Prediction of multipactor breakdown thresholds in coaxial transmission lines for traveling, standing, and mixed waves," *IEEE Plasma Sci.*, vol. 37, no. 10, pp. 2031–2040, Oct. 2009.

[16] V. E. Semenov, E. Rakova, A. Sazontov, *et al.*, "Simulations of multipactor thresholds in shielded microstrip lines," *J. Phys. D, Appl. Phys.*, vol. 42, no. 20, Sep. 2009, Art. no. 205204.

[17] P. Gonzalez, C. Alcaide, R. Cervera, *et al.*, "Multipactor threshold estimation techniques based on circuit models electromagnetic fields and particle simulators," *IEEE J. Microw.*, vol. 2, no. 1, pp. 57–77, Jan. 2022.

[18] H. Fenech, S. Amos, A. Tomatis, and V. Soumpholphakdy, "High throughput satellite systems: An analytical approach," *IEEE Trans. Aerosp. Electron. Syst.*, vol. 51, no. 1, pp. 192–202, Jan. 2015.

[19] J. Christensen, "ITU regulations for Ka-band satellite networks," in *Proc. 30th AIAA Int. Commun. Satell. Syst. Conf. (ICSSC)*, Sep. 2012, p. 15 179. [Online]. Available: https://arc.aiaa.org/doi/abs/10.2514/6.2012-15179.

[20] E. Rajo-Iglesias and P.-S. Kildal, "Groove gap waveguide: A rectangular waveguide between contactless metal plates enabled by parallel-plate cut-off," in *Proc. 4th Eur. Conf. Antennas Propag.*, Barcelona, Spain, Apr. 2010, pp. 1–4.

[21] L. Wu, Y. Wu, Y. Yao, R. Huang, Z. Xu, and W. Wang, "Dual-band bandpass filter with controllable transmission zeros using multimode GGW cavity," *IEEE Microw. Wireless Technol. Lett.*, vol. 34, no. 7, pp. 891–894, Jul. 2024.

[22] M. Malki, L. Yang, and R. Gomez-Garcia, "Sharp-rejection in-line groove-gap-waveguide bandpass filter with multiple transmission zeros for ku-band application," *IEEE Microw. Wireless Technol. Lett.*, vol. 34, no. 5, pp. 478–481, May 2024.

[23] Q. Li, D. Guo, J. Mou, J. Li, and K.-D. Xu, "Groove gap waveguide bandpass filter based on spoof surface plasmon polariton for ka-band applications," *IEEE Trans. Microw. Theory Tech.*, vol. 72, no. 1, pp. 340–347, Jan. 2024.

[24] Z. Liu, J.-Y. Deng, and D. Sun, "Slow-wave groove gap waveguide bandpass filter," *IEEE Access*, vol. 7, pp. 52 581–52 588, 2019.

[25] S. Marini, M. F. Rocher, A. M. Hernández, E. G. Nieves, A. J. López, and V. E. Boria, "Ka-band diplexer design based on half-mode groove gap waveguide," *Int. J. Electron. Commun.*, vol. 175, no. 1, pp. 1434–8411, Feb. 2024.

[26] P.-S. Kildal, E. Alfonso, A. Valero-Nogueira, and E. Rajo-Iglesias, "Local metamaterial-based waveguides in gaps between parallel metal plates," *IEEE Antennas Wireless Propag. Lett.*, vol. 8, pp. 84–87, 2009.

[27] E. Rajo-Iglesias and P. S. Kildal, "Numerical studies of bandwidth of parallel-plate cut-off realised by a bed of nails, corrugations and mushroom-type electromagnetic bandgap for use in gap waveguides," *IET Microw., Antennas Propag.*, vol. 5, no. 3, pp. 282–289, Feb. 2011.

[28] A. Berenguer, D. Sánchez-Escuderos, B. Bernardo-Clemente, M. Baquero-Escudero, and V. E. Boria, "Groove gap waveguide as an alternative to rectangular waveguide for H-plane components," *Electron. Lett.*, vol. 52, no. 11, pp. 939–941, May 2016.

[29] A. Morales-Hernández, M. Á. Sánchez-Soriano, M. Ferrando-Rocher, S. Marini, and V. E. Boria, "In-depth study of the corona discharge breakdown thresholds in groove gap waveguides and enhancement strategies for inductive bandpass filters," *IEEE Access*, vol. 10, pp. 129 149–129 162, 2022.

[30] J. Vague, I. Asensio, Á. Coves, *et al.*, "Study of the multipactor effect in groove gap waveguide technology," *IEEE Trans. Microw. Theory Tech.*, vol. 70, no. 5, pp. 2566–2578, May 2022.

[31] European Space Agency and Val Space Consortium High-Power Laboratories, [Online]. Available: http://www.val-space.com.

[32] CST Microwave Studio, Accessed on: 2025-06-16, [Online]. Available: https://www.3ds.com/products/simulia/cst-studio-suite.

[33] A. Berenguer, Á. Coves, F. Mesa, E. Bronchalo, and B. Gimeno, "Analysis of multipactor effect in a partially dielectric-loaded rectangular waveguide," *IEEE Trans. Plasma Sci.*, vol. 47, no. 1, pp. 259–265, Jan. 2019.

[34] A. Berenguer, Á. Coves, B. Gimeno, E. Bronchalo, and V. E. Boria, "Experimental study of the multipactor effect in a partially dielectric-loaded rectangular waveguide," *IEEE Microw. Wireless Compon. Lett.*, vol. 29, no. 9, pp. 595–597, Sep. 2019.

[35] "Multipacting design and test," European Cooperation for Space Standardization (ECSS), ESA-ESTEC, Amsterdam, The Netherlands, ECSS-E-ST-20-01C, Jun. 2020, ESA Publication Division.

[36] S. Cogollos, J. Vague, V. E. Boria, and J. D. Martínez, "Novel planar and waveguide implementations of impedance matching networks based on tapered lines using generalized superellipses," *IEEE Trans. Microw. Theory Techn.*, vol. 66, no. 4, pp. 1874–1884, Apr. 2018.